www.serd.ait.ac.th/reric

ANFIS based Coordination of Multiple UPFC Control Functions for Damping Low Frequency Oscillations in Power Systems

M. Sobha*[1], R.S. Kumar* and S. George*

Abstract – *Multiple controllers perform the control functions of unified power flow controller (UPFC) to exploit its various functional capabilities. Due to dynamic interactions among different UPFC controllers, performance is deteriorated when separately designed and individually implemented stable UPFC controllers are in joint operation. An adaptive neuro-fuzzy inference system (ANFIS) based supplementary unified power flow controller (UPFC) in co-ordination with other controllers of the UPFC to damp the low frequency oscillations is proposed in this paper. A hybrid learning procedure was adopted for the proposed ANFIS to adapt the gains of the damping controller over wide range of operating conditions, various control signals and in presence of different UPFC controllers. The input to the fuzzy controller was the deviation in the generator angular speed and output, the control signal to be superimposed on the selected UPFC signal. The performance of the proposed adaptive damping controller was validated by time domain simulation under varying operating conditions, system parameters and in presence of other UPFC controllers.*

Keywords – ANFIS, co-ordination, hybrid learning, multiple controllers, UPFC.

1. INTRODUCTION

Application of high power electronic devices has made the concept of FACTS feasible for power flow control, voltage control and additionally for enhancing the damping of low frequency electromechanical oscillations. This technology has paved way for improved utilization of existing transmission capabilities by providing fast and continuous control of power flow through the transmission system [1]. The unified power flow controller, a multifunctional FACTS controller opens up new opportunities for controlling power and maximizing the utilization of existing transmission systems [2]. The salient feature of UPFC is its multiple control functions where the series and shunt part of the UPFC can be equipped with various controllers. To compensate for the active power exchange of the UPFC with the power system and to maintain it to zero at steady state operating condition, the DC voltage across the DC link capacitor needs to be controlled by a DC voltage regulator [2]–[5]. Assignment of individual control input-output pairs for each of these control function may perform well when implemented individually, but is likely to result in deteriorating performance when in joint operation due to lack of co-ordination between the various control signals [6].

Tambey and Kothari [7] have presented systematic design of supplementary UPFC damping controller in the UPFC control system for damping the electromechanical mode oscillations with four alternative UPFC damping controllers. However, interaction of these controls signals with other UPFC control channels and the resulting performance has not been analyzed. In [8], these authors have presented the interactions of the UPFC damping controllers with other control signals. Wang [6] has presented multiple-input multiple-output control system for co-ordination of various UPFC control channels. The gains of these controllers are designed on the basis of nominal operating conditions, which remain independent of system operating conditions and line loadings. An adaptive UPFC supplementary damping controller has been presented in [9], but the performance of the designed controller has not been validated in joint operation with other UPFC control channels.

This work proposes an adaptive fuzzy inference system (ANFIS) based co-ordination of UPFC supplementary damping controller with other controllers of UPFC for damping the power system electromechanical oscillations. The adaptive fuzzy controller is obtained by embedding the fuzzy inference system into the framework of adaptive networks [10]. The linguistic rules, considering the dependence of the plant output on the controlling signal, are used to build the initial fuzzy inference structure. The fuzzy parameters of the adaptive controller are trained by the batch hybrid learning rule using the training data obtained from conventional design under widely varying system and load conditions with the selected UPFC control signals (based on modulating indices and voltage phase angles of UPFC series and shunt converters) and in the presence of different UPFC control channels.

2. DESIGN OF UPFC CONTROLLERS

This section presents the design of three different UPFC controllers namely, DC voltage regulator (DVR), power flow controller (PFC) and power oscillation damping controller (POD). The arrangement of the power system including the UPFC incorporated with these controllers is shown in Figure 1.

These controllers are designed and tested on a single-machine infinite-bus system installed with UPFC [11] shown by Figure 2. The UPFC consists of an excitation transformer (ET), a boosting transformer (BT), two three-phase GTO based voltage source converters and DC link capacitor. The excitation system is assumed to be

* Department of Electrical Engineering, National Institute of Technology Calicut, 673 601, Kerala, India.

[1] Corresponding author;
E-mail: sobha_kumar1@rediffmail.com.

of type IEEE-ST1A [12]. The various choices of control signals of UPFC are modulating index of series converter (m_B), modulating index of shunt converter (m_E), phase angle of series converter voltage (δ_B) and phase angle of shunt converter voltage (δ_E).

The overall model of the generator, exciter, the power system and the UPFC with controllers are given by:

$$\dot{x}(t) = f(x(t), u(t)) \tag{1}$$

For the design of the various UPFC controllers shown in Figure 1, the nonlinear equations representing the system given by Equation 1 are linearized around a nominal operating point and the equations so obtained are given by Equation 2.

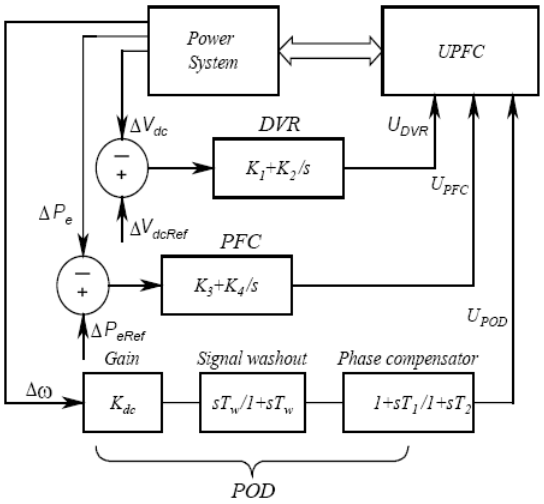

Fig. 1. Multicontroller incorporated UPFC installed power system.

$$\begin{bmatrix} \dot{\Delta\delta} \\ \dot{\Delta\omega} \\ \dot{\Delta E'q} \\ \dot{\Delta E_{fD}} \\ \dot{\Delta v_{dc}} \end{bmatrix} = \begin{bmatrix} 0 & \omega_0 & 0 & 0 & 0 \\ -K_1/M & -D/M & -K_2/M & 0 & -K_{p1}/M \\ -K_4/\dot{T}_{do} & 0 & -K_3/\dot{T}_{do} & 1/\dot{T}_{do} & -K_{q1}/\dot{T}_{do} \\ -K_A K_5/T_A & 0 & -K_A K_6/T_A & -1/T_A & -K_A K_{v1}/T_A \\ K_7 & 0 & K_8 & 0 & -K_9 \end{bmatrix} \times \begin{bmatrix} \Delta\delta \\ \Delta\omega \\ \Delta E'_q \\ \Delta E_{fD} \\ \Delta v_{dc} \end{bmatrix} + \begin{bmatrix} 0 & 0 & 0 & 0 \\ -K_{pe}/M & -K_{p\delta e}/M & -K_{pb}/M & -K_{p\delta b}/M \\ -K_{qe}/\dot{T}_{do} & -K_{q\delta e}/\dot{T}_{do} & -K_{qb}/\dot{T}_{do} & -K_{q\delta b}/\dot{T}_{do} \\ -K_A K_{ve}/T_A & -K_A K_{v\delta e}/T_A & -K_A K_{vb}/T_A & -K_A K_{v\delta b}/T_A \\ K_{ce} & K_{c\delta e} & K_{cb} & K_{c\delta b} \end{bmatrix} \times \begin{bmatrix} \Delta m_E \\ \Delta\delta_E \\ \Delta m_B \\ \Delta\delta_B \end{bmatrix} \tag{2}$$

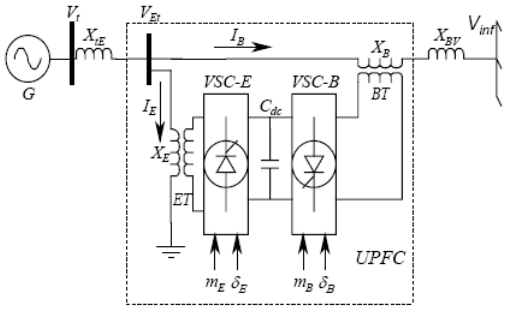

Fig. 2. UPFC installed in single-machine infinite bus power system.

These UPFC controllers are designed separately without considering the dynamic interactions among the three input–output channels, where the multifunctional UPFC is treated as a single- input single-output system. Proportional plus Integral control law [13] is used for the design of DVR and PFC controllers and the POD controller is designed using the phase compensation method [14].

2.1. Design of UPFC DC Voltage Regulator (DVR)

Maintaining constant dc link voltage is a basic control requirement for the UPFC control system. The dc link voltage varies when shunt converter compensates for the real power exchange (positive or negative) of the series converter with respect to the system, ensuring zero real power exchange between the UPFC and the power system in steady state. For the design of the voltage regulator, the linearized model of the system given in Figure 2 is considered.

The linearization parameters calculated for the selected operating point given in Appendix B. The input signal to the controller is the error between the change in DC link voltage and change in set reference value. The output control signal of the UPFC voltage regulator

(ΔU_{DVR}) is chosen among the four control signals of series and shunt converter VSC of UPFC, $\Delta m_{E,}$ $\Delta m_{B,}$ $\Delta\delta_E$ and $\Delta\delta_B$ .The proportional and integral gains K_1 and K_2 are tuned for these four output control signals using Ziegler-Nichols tuning method [15]. Among these control signals, the most appropriate output control signal is chosen by comparing the results of eigen value analysis with the four output control signals given in Table 1. On examination of the eigen values of the system considered with the various UPFC control signals, it is evident that control signal $\Delta\delta_E$ (phase angle of shunt converter voltage) is resulting in better damping contribution for the electromechanical mode when compared to other signals. Thus $\Delta U_{DVR} = \Delta\delta_E$ is chosen as the output control signal for the UPFC DC voltage regulator in further analysis. The corresponding proportional and integral gains are K_1=2 and K_2 =1 respectively.

Table 1. Eigen values of UPFC installed SMIB system incorporated with DVR.

Control Signal	$\Delta\delta_B$	$\Delta\delta_E$	Δm_E	Δm_B
Eigen Values	-92.612	-92.64	-92.59	-92.622
	0.0628± 8.020i[a]	-0.037± 8.0613i[a]	0.211± 7.9843i[a]	-0.008± 8.0306i[a]
	-8.0624	-7.8645	-8.2410	-7.9754
	0.9347	0.4827	-0.1211	-0.2973

[a] electromechanical mode

2.2 Design of UPFC DVR

In the power flow control mode, the UPFC output voltage is controlled so as to result in desired real and reactive power flow in the line. The Proportional Integral controller for the UPFC power flow controller is designed based on the linearized model of the system given in Figure 2. The design is carried out at the same operating condition as in the case of DVR and the linearization parameters are given in Appendix B. The error between the change in active power and the change in reference power setting is chosen as the input to the controller. The output control signal (ΔU_{PFC}) are the various UPFC control signals namely $\Delta m_{E,}$ Δm_B $\Delta\delta_E$ and $\Delta\delta_B$. The proportional and integral gains K_3 and K_4 are tuned for these four output control signals using Ziegler-Nichols tuning method and the most appropriate output control signal is chosen by comparing the results of system eigen value analysis with the four output control signals given in Table 2.

Table 2. Eigen values of UPFC installed SMIB system incorporated with PFC.

Control Signal	$\Delta\delta_B$	$\Delta\delta_E$	Δm_E	Δm_B
Eigen Values	-92.645	-92.787	-91.838	-90.730
	-0.528± 4.115i[a]	-0.018± 7.381i[a]	-0.506 ± 6.153i[a]	-0.754± 5.681i[a]
	-8.0137	-7.9706	8.4110	-9.0778
	-0.0042	-0.0041	-0.0041	-0.0041

[a] electromechanical mode

In this case, control signal Δm_B (modulating index of series converter voltage) is chosen on the basis of better contribution of this control signal to damping of the electromechanical mode of the system. Hence further analysis is done by choosing $\Delta U_{PFC} = \Delta m_B$ as the output control signal for the UPFC power flow controller. The corresponding proportional and integral gains are K_3 =2 and K_4 =0.2, respectively.

2.3 Design of UPFC POD

The UPFC is installed for the purpose of multiple control functions, one of which is the suppression of low-frequency oscillations occurring in the power system. To improve the damping performance of UPFC, a supplementary damping controller is installed to superimpose the damping function on the UPFC control signal. The input to the controller is $\Delta\omega$, the change in the generator angular speed and the output is ΔU_{POD}, the damping control signal. The output control signal (ΔU_{POD}) is based on modulation of the various UPFC signals namely $\Delta m_{E,}$ $\Delta m_{B,}$ $\Delta\delta_E$ and $\Delta\delta_B$ as in the case of DVR and PFC. The structure of POD consists of gain, signal washout and phase compensator circuits as shown in Figure 1. The gain settings and time constants for the damping controller are calculated by phase compensation technique. The value of the washout time constant, T_w is taken as 10 s. The controller is designed for the four alternative choices of UPFC control signals. From the results of the eigen value analysis given in Table 3, the most important control signals from the viewpoint of damping of electromechanical mode of the system become $\Delta\delta_E$ and $\Delta\delta_B$. These signals are selected as the output control signals (ΔU_{POD}) for further studies. The controller parameters for the selected signals are as given in Table 4.

Table 3. Eigen values of UPFC installed SMIB system incorporated with POD.

Control Signal	$\Delta\delta_B$	$\Delta\delta_E$	Δm_E	Δm_B
Eigen Values	-92.557	-92.728	-92.6118	-92.612
	-2.795 ± 7.410i[a]	-2.955 ± 8.3846i[a]	-1.048 ± 7.8108i[a]	-1.048 ± 7.8108i[a]
	-8.6269	-7.6317	-8.0652	-8.0652
	-0.1016	-0.1007	-0.1020	-0.1020

Table 4. Parameters of POD controllers.

Controller parameters ↓ / UPFC Control signals →	K_{dc}	T_1(s)	T_2 (s)
$\Delta\delta_E$	116.76	0.1308	0.1210
$\Delta\delta_B$	425.46	0.1216	0.1300

3. INTERACTION BETWEEN UPFC CONTROL SIGNALS

Three different input-output control pairs individually designed, without considering their interactions, as

presented in Section 2 are utilized for the different functions of UPFC. In real time, these controllers are assigned to take up their control action in joint operation, which is likely to deteriorate the overall performance. The impact of these interactions upon the damping of low frequency oscillation of the system is analyzed in this paper. Figure 3a compares the response of selected output control signals for DVR and POD for a step rise of 1% at the time instant t = 0.5 second to the mechanical input of the power system shown in Figure 1. The control signals are $\Delta U_{POD}=\Delta\delta_B$ *or* $\Delta\delta_E$ and $\Delta U_{DVR}=\Delta\delta_E$. In Figure 3b similar comparisons are presented for the PFC and POD control channels where the control signals chosen are $\Delta U_{POD}=\Delta\delta_B$ *or* $\Delta\delta_E$ and $\Delta U_{PFC}=\Delta m_B$. From these figures, it is evident that the signals are less co-operating when the output control signal of POD (ΔU_{POD}) is $\Delta\delta_B$ for the case of joint operation with DVR as well as with PFC control channels. To examine the impact of these interactions upon the dynamic performance of the system, the following cases are considered.

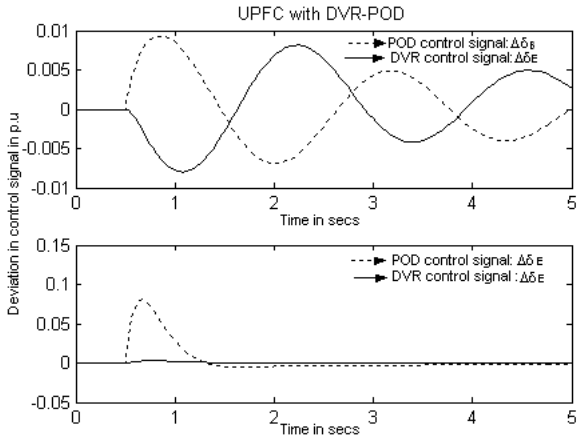

Fig. 3a. Output control signals of DVR and POD.

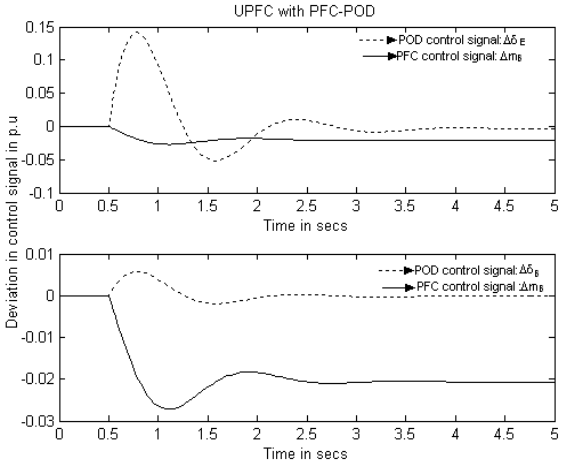

Fig. 3b. Output control signals of PFC and POD.

3.1. Interaction between POD and DVR Control Channels

The DVR and POD control channels are assumed to be functioning jointly for the power system installed with UPFC shown in Figure 1. By choosing the control signal for DVR as $\Delta\delta_E$ and POD as $\Delta\delta_B$ *or* $\Delta\delta_E$, the shunt part of UPFC is equipped with DC voltage regulation function and series or shunt voltage angles for power oscillation damping support. The test system in Figure 2 is subjected to a step rise of 0.01p.u in the mechanical power input of the machine at the time instant t = 0.5 second when the machine is operating in the nominal operating conditions as listed in Appendix A. Figure 4 compares the variation of $\Delta\omega$ of the synchronous machine for UPFC with the POD controller alone with that of the case when POD and DVR controllers are in joint operation. From Figure 4, it is evident that the system performance has deteriorated when the two controllers are in joint operation. As evident from this figure, the result shows more oscillatory response with control signal $\Delta U_{POD}=\Delta\delta_B$ as compared to $\Delta\delta_E$ due to lesser co-operation of this signal with DVR control signal. These results coincide with the inferences given in section 3 based on results presented in Figure 3.

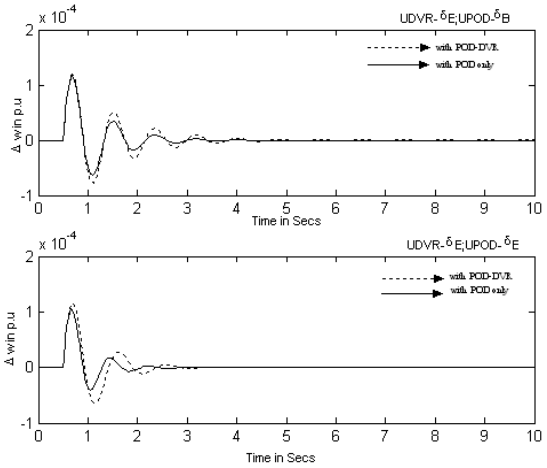

Fig. 4. Comparison of Δω variations with POD alone and POD-DVR in joint operation. $\Delta U_{POD}=\Delta\delta_B, \Delta\delta_E$.;$\Delta U_{DVR}=\Delta\delta_E$

3.2 Interaction between POD and PFC Controller

To investigate the effect of PFC and POD controller interaction upon the damping of low frequency oscillations of the system it is assumed that the PFC and POD control channels are in operation. The series part of UPFC is equipped to support the power flow control by choosing the control signal of PFC as Δm_B and series or shunt voltage angles are controlled for power oscillation damping by selecting $\Delta\delta_B$ or $\Delta\delta_E$ as POD control signals. The test system in Figure 2 is subjected to a step rise of 0.01p.u in the mechanical power input of the machine at the time instant t = 0.5 second when the machine is operating in the nominal operating conditions. Figure 5 compares the variation of $\Delta\omega$ of the synchronous machine with the POD controller alone and with POD and PFC controllers in joint operation.

As in the case of joint operation of DVR and POD, Figure 5 shows that the performance has deteriorated for the system when the two controllers are in joint operation. The result shows more oscillatory response with control signal $\Delta U_{POD}=\Delta\delta_B$ as compared to $\Delta\delta_E$ due to lesser co-operation of this signal with PFC control signal. The results presented in Sections 3.1 and 3.2 indicate the existence of negative dynamic interactions between the

various control loops with different control objectives. An adaptive fuzzy co-ordination method is proposed in this paper for the co-ordination of the POD control signal with respect to the DVR and the PFC control signals.

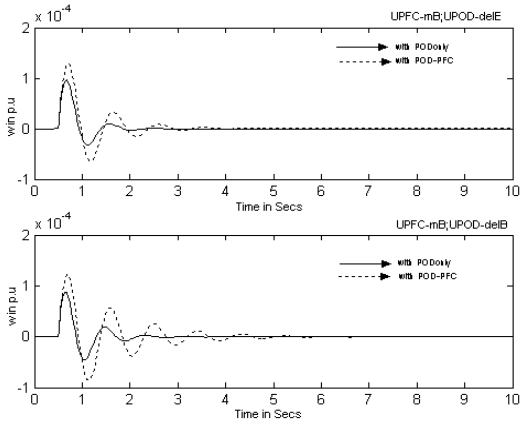

Fig. 5 Comparison of Δω variations with POD alone and POD-PFC in joint operation $\Delta U_{POD}=\Delta\delta_B$, $\Delta\delta_E$; $\Delta U_{PFC}=\Delta m_B$

4. DESIGN OF PROPOSED POD CONTROLLER

In order to co-ordinate the POD controller with other controllers under different operating conditions an adaptive fuzzy POD controller is proposed. The adaptive fuzzy controller is obtained by embedding the fuzzy inference system into the framework of artificial neural networks. The design procedure for the proposed adaptive neuro-fuzzy inference system (ANFIS) based POD controller consists of:

- Determination of initial fuzzy structure.
- ANFIS training of the initial fuzzy structure for updating the fuzzy parameters to meet the desired control performance.
- Evaluation of the performance of the ANFIS controller

4.1 Determination of Initial Fuzzy Structure

The input to the proposed fuzzy inference system is taken as the deviation in the generator angular speed ($\Delta\omega$) and the output as the damping control signal (ΔU_{POD}). The linguistic rules, considering the dependence of the plant output on the controlling signal, are used to build the initial fuzzy inference structure. The input signal is fuzzified using seven fuzzy sets A_i; *i=1 to 7*.The membership functions (MF's) chosen for the input set is the generalized bell-shaped function with maximum equal to 1 and minimum equal to 0 and is given by:

$$\mu A_i(X)=\frac{1}{1+\left|\frac{x-c_i}{a_i}\right|^{2b_i}}, i=1 \quad to \quad 7 \tag{3}$$

where $\{a_i, b_i, i_i\}$ is the premise parameter set. The initial values of premise parameters are set in such a way that the MF's are equally spaced in the range [-1 1]. The rule base with seven fuzzy if-then rules of (TS) Takagi and Sugeno's type [16] given by:

If $\Delta\omega_i$ *is* A_i, *then* Δu_i *is* $p_i x+r_i$; *I =1 to 7* (4)

The output control signal of the POD controller ΔU_{PODi}, is calculated by the linear combination of the inputs and $\{p_i, r_i\}$ denote the consequent parameter set. Table 5 shows the premise parameters initially chosen and the resulting consequent parameters generated based on the rule base and membership function. These parameters are updated by ANFIS training presented in Section 4.2. However the seven rules of the initial fuzzy structure remain unchanged during the adaptation process.

Table 5. Initial premise and consequent parameters.

Parameters → / MF's ↓	a_i	b_i	c_i	p_i	r_i
A_1	0.1667	2.5	-1	0	0
A_2	0.1667	2.5	-0.6666	0	0.1666
A_3	0.1667	2.5	-0.3334	0	0.3333
A_4	0.1667	2.5	0	0	0.5
A_5	0.1667	2.5	0.3334	0	0.6666
A_6	0.1667	2.5	0.6666	0	0.8333
A_7	0.1667	2.5	1	0	1

4.2 ANFIS Training

The steps for ANFIS training to adapt the initial fuzzy premise parameters for construction of the proposed optimum input output pattern to perform the desired control action is presented.

i. Selection of the network architecture

A four layer feed forward network architecture is selected for the ANFIS based damping controller as shown in Figure 6.The node functions of the various layers of ANFIS for the adjustments of premise parameter set $\{a_i, b_i, c_i\}$ are as follows.

Layer1: Adaptive node function with premise parameter set $\{a_i, b_i, c_i\}$ input:

$$O_i^1 = \mu A_i(X); I = 1 \text{ to } 7 \tag{5}$$

X input to node i, ; A_i linguistic label associated the node; O_i degree to which the given X satisfies the quantifier A_i;

Layer 2: Fixed node function:

$$\varpi = \omega_i \Big/ \sum_{i=1}^{7} \omega_i \tag{6}$$

ω_i firing strengths of each rule ; ϖ_i normalized firing strengths for the output function.

Layer 3: Adaptive node function

$$O_i^3 = \varpi_i f_i = \varpi_i (p_I X + r_i); i = 1 \text{ to } 7 \tag{7}$$

where $\{p_i, r_i\}$ consequent parameter set.

Layer 4: Fixed node function

$$O_i^4 = \sum_{i=1}^{7} \varpi_i f_i = \sum_{i=1}^{7} (p_i X + r_i) \tag{8}$$

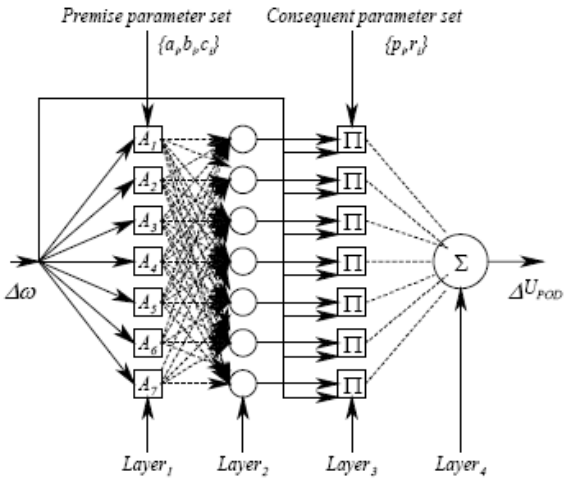

Fig. 6. Proposed ANFIS architecture.

ii. Selection of learning algorithm

The choice of learning algorithm is based on trade-off between computation complexity and resulting performance. The learning method adopted in this paper is the hybrid learning rule combining the learning rule based on the gradient descent method and the Least Square Error (LSE) method [10]. This hybrid learning technique speeds up the learning process compared to the gradient method alone, which exhibits the tendency to become trapped in local minima.

Each epoch of this hybrid learning procedure is composed of a forward pass and backward pass. In the forward pass the training data is presented and the functional signals proceed forward to calculate each node output.The consequent parameters are identified and error measure is calculated. In the backward pass, the error rates propagate from the output end toward input end and the premise parameters are updated by gradient method. The update action on premise parameters takes place only after the whole training data set is presented thus adopting batch learning paradigm for the learning algorithm. Steps to demonstrate the use of the hybrid-learning algorithm for training ANFIS are given below:

a. Initialization

- Load input vector $[\Delta\omega_j \; \Delta u_{PODj}]$; *j=1to P, P the number of training pairs used*
- Select MF A_i; *i=1 to7*
- Initialize premise parameter matrix $\{a_i \; b_i \; c_i\}$ for Generalized Bell membership
  a=half width of bell function, b-slopes at crossover point (where MF=0.5), c=center of corresponding membership function
- Select *SSE* goal =0. 3; learning rate η=0.5

b. Forward pass

- Layer 1:Generate membership grades; $A_i = [\Delta\omega_j(a_i \; b_i \; c_i)]$
- Layer 2: Generate firing strengths $\omega_i=A_i$; *i=1 to 7*
- Layer 3: Normalize firing strengths $\varpi_I = \omega_I / \sum\omega_I$; *i=1 to 7*
- Compute consequent parameters (*C_params)*, $\{p_i,r_i\}$; *i=1 to 7* using LSE algorithm as $\Delta u_{inner} = [\varpi_I \times \Delta\omega_j]$; *i=1 to 7*

c. Backward pass

- Estimate the error gradient vectors using gradient descent algorithm of hybrid learning rule
- Calculate output error as $e=y-\Delta u_j$
- Calculate SSE as SSE=sum (sum (e.^2)); If SSE< SSE goal stop training. Else,
- Propagate derivative of error measure with respect to each node in the four layers
- Compute $\partial E/\partial [a_i \; b_i \; c_i]$ overall error measure with respect to each premise parameter
- Update premise parameters as:

$$\Delta[a_i \; b_i \; c_i] = - \eta \times \partial E/\partial[a_i \; b_i \; c_i]$$

$$[a_i \; b_i \; c_i]_{new} = [a_i \; b_i \; c_i] + \Delta [a_i \; b_i \; c_i]$$

iii. Generation of training data

The proposed fuzzy structure has 21 premise parameters, 14 consequent parameters, thus in total there are 35 parameters to be estimated with their initial values as given in Table 5. The input-output patterns required for the training of the ANFIS to adapt these parameters is generated as follows.

a. Training data for adaptation to various operation situations

Using phase compensation technique given in section 2, design the conventional POD controller at various operating conditions and system parameters. Generate $(\Delta\omega, \; \Delta U_{POD})$ training pairs from the constant gain controller so designed. In this paper a finite set of power system operating range is so chosen so as to encompass all practical situations as:

$$\{P_e, \; Q_e \text{ , and } X_e\} = \{0.1\text{- } 1.2, \; 0.01\text{- } 0.4, \; 0.3\text{- } 0.9\}$$

where P_e is active power, Q_e is reactive power and $X_e$is the system equivalent reactance all in per unit.

b. Training data for co-ordination

At the first level, the training is done to learn the POD-DVR control channel coordination. The training data is generated by repeating step a on inclusion of DVR control loop along with POD control channel in the system. At the second level, training is done to learn the POD-PFC control channel. For this the DVR control loop is made open and PFC control loop is included along with the POD control channel. Step a is again repeated to generate the input output control pairs.

c. Training data for adaptation to various control signals

Steps a and b are repeated for the two cases of output control signals selected for the POD control loop, namely $\Delta U_{POD}=\Delta\delta_B$ *and* $\Delta\delta_E$.

The adaptive network is trained using the training data generated and the hybrid-learning algorithm. The distribution of initial fuzzy subset of the seven MF's (A_1

to A_7) in the universe of discourse of input function $\Delta\omega$ is equally spaced in the range [-1 1]. Figure 7 shows the initial input membership functions and the input membership functions of the resulting fuzzy inference system after 40 training epochs when the error reduced to 0.3. From the figure it can be seen that the membership functions have moved towards the origin and these changes are more for the middle membership functions due to the sharper changes of the training data around the origin. The corresponding premise and the consequent parameters are given in Table 6.

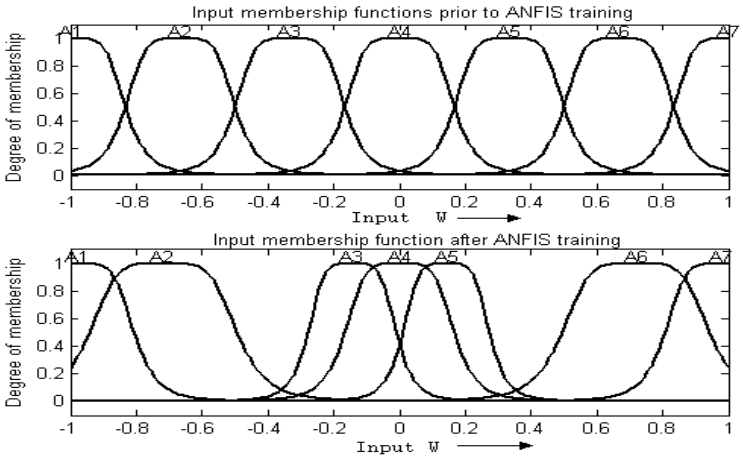

Fig. 7. Membership functions prior to and after ANFIS training.

Table 6. Final premise and consequent parameters.

Parameters → / MF's ↓	a_i	b_i	c_i	p_i	r_i
A_1	0.1721	2.500	-0.978	-2.186	-2.111
A_2	0.225	2.500	-0.718	-0.266	3.6333
A_3	0.134	2.518	-0.144	3.237	-6.417
A_4	0.167	2.500	-1.642	6.863	-0.332
A_5	0.132	2.518	0.1414	3.264	6.5055
A_6	0.225	2.500	0.7182	-0.260	-3.637
A_7	0.172	2.501	0.9783	-2.188	2.114

4.3. Simulation results

ANFIS training is done to learn a good co-ordination between the POD-DVR and POD-PFC control channels in presence of varying parameter and system-loading conditions with selected output control signals. The performance evaluation of the designed ANFIS based POD controller for coordination with other controllers is done by conducting time domain simulations for the system given in Figure 1 in presence of DVR and PFC control channels considered separately with the chosen control output signals namely $\Delta U_{DVR}=\Delta\delta_E$ *and* $\Delta U_{PFC}=\Delta m_B$. The results are compared with constant gain POD controller designed using phase compensation technique at selected operating conditions. Investigations are repeated for each of the POD control signal considered namely $\Delta U_{POD}=\Delta\delta_E$ *and* $\Delta\delta_B$ under various operating conditions as follows:

i. Case 1. UPFC with POD and DVR controllers

For the system shown in Figure 1, a step rise of 0.01p.u in the mechanical power input of the machine is initiated at the time instant t = 0.5 second when the machine is operating in the nominal operating conditions. The POD controller is installed to achieve the control function of compensating for the power mismatch in the system due to the disturbance and the DVR controller has the function of maintaining the DC link voltage to have zero real power exchange with the system under steady state. Figure 8 shows the variation of $\Delta\omega$ of the synchronous machine with the ANFIS based POD controller and also with the constant gain POD controller when DVR is in the closed loop. These results are compared when the system is operating without the DVR controller. Simulation results with the two choices of POD control signal, $\Delta U_{POD}=\Delta\delta_E$ *and* $\Delta\delta_B$ are shown in the Figure 8. From the results it is evident that the ANFIS based controller performance is better than the constant gain controller when the two controllers are in joint operation. It is also observed that the response is improved in the case of ANFIS based controller when $\Delta U_{POD}=\Delta\delta_E$.

The effectiveness of the ANFIS based POD controller with DVR is examined for the control function of the DVR control channel. Simulation is done with step rise of 0.01 p.u in mechanical power input of the machine at the time instant t = 0.5 second when the machine is operating in the nominal operating conditions. The time domain variations of ΔV_{dc} of the system for a step rise of 0.01 p.u to the dc reference voltage are presented in Figure 9. The figure compares the ΔV_{dc} variations with $\Delta U_{POD}=\Delta\delta_E$ *and* $\Delta\delta_B$ for the constant gain and ANFIS trained controllers. With $\Delta U_{POD}=\Delta\delta_B$ the result indicates that the performance of DVR controller has not

deteriorated with the ANFIS training of the POD controller and with $\Delta U_{POD}=\Delta\delta_E$, DVR with ANFIS trained POD is showing lesser overshoot and thus better performance.

To evaluate the robustness of the proposed controller to system changes and parameter variations, exhaustive investigations are carried out and the typical results are shown in Figures 10 and 11. Figure 10 shows the variations of $\Delta\omega$ of the synchronous machine with POD-DVR controllers in joint operation and also with ANFIS based POD-DVR controllers when the system is operating at light load condition where P_e and Q_e values are lower than the nominal conditions. The figure compares the performance of the system with these controllers with the results obtained with POD alone. It is evident that the ANFIS based controller is showing improved performance for both the U_{POD} control signals considered. In Figure 11 similar responses are shown with the equivalent reactance higher than the nominal value. It is observed that the system is showing undamped oscillations for this condition when POD-DVR controllers are in joint operation. However even in this condition the ANFIS trained POD controller performance is appreciable which establishes the robustness of the proposed controller to system and parameter variations.

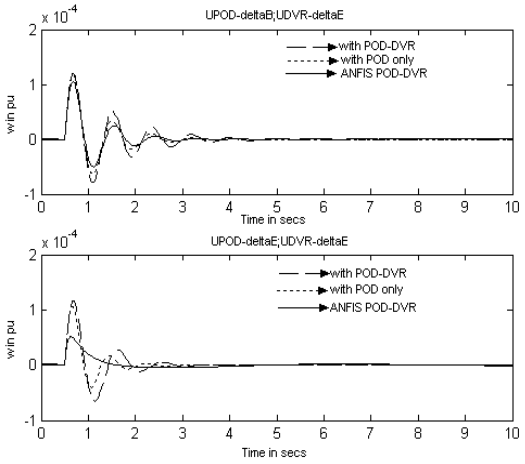

Fig. 8. Comparison of $\Delta\omega$ variations for step change in mechanical power input.

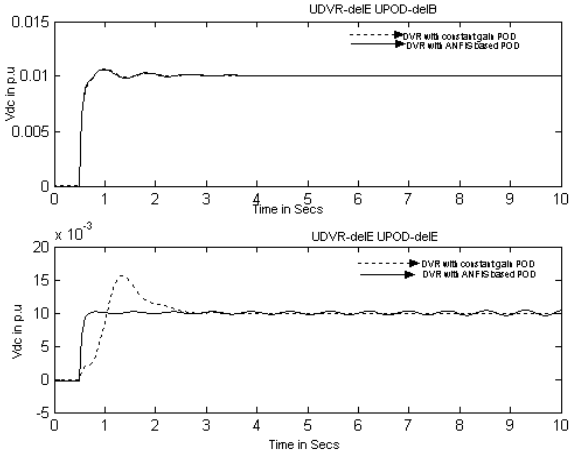

Fig. 9. ΔV_{dc} variations for step change in V_{dcref}.

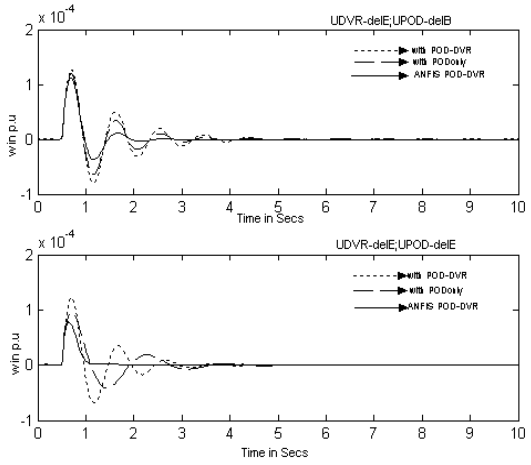

Fig. 10. Comparison of $\Delta\omega$ variations for step change in mechanical power input *Pe=0.2p.u;Qe=0.01p.u ;Xe=0.5p.u*

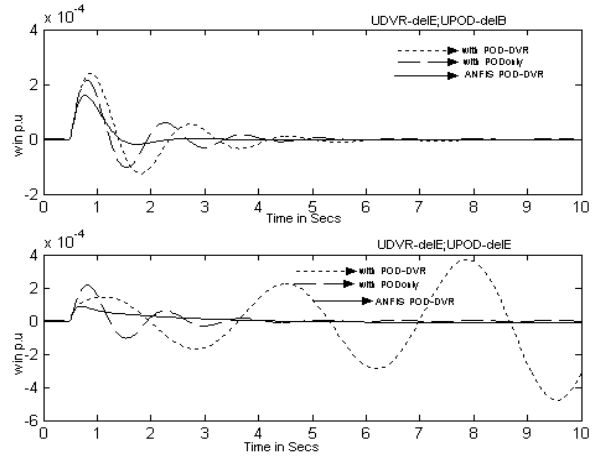

Fig. 11. Comparison of $\Delta\omega$ variations for step change in mechanical power input *Pe=0.6p.u;Qe=0.1p.u; Xe=0.9p.u*

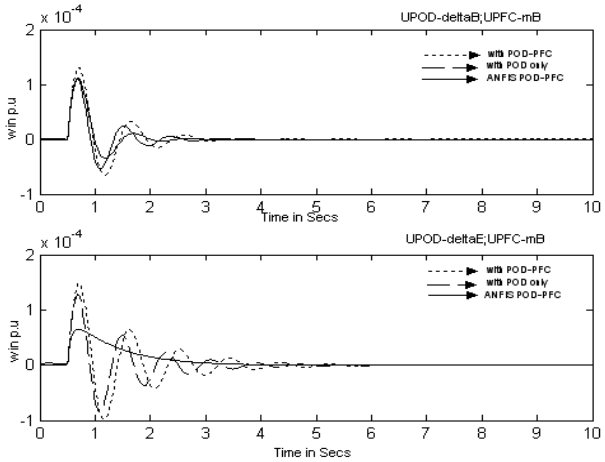

Fig. 12. Comparison of $\Delta\omega$ variations for step change in mechanical power input.

ii. Case 2. UPFC with POD and PFC controllers

To investigate the performance of the proposed controller in joint operation with the PFC controller, it is assumed that the DVR controller shown in Figure 1 is not operating and the PFC controller is included in the closed loop with the POD controller. The POD controller is installed to achieve the control function of compensating for the power mismatch in the system due to the disturbance and the PFC controller has the function of controlling real power flow through the line according to set the reference value. As in Case 1 for the system shown in Figure 1, a step rise of 0.01p.u in the mechanical power input of the machine is initiated at the time instant t = 0.5 second when the machine is operating in the nominal operating conditions. The Figure 12 shows the variation of $\Delta\omega$ of the synchronous machine with the ANFIS based POD controller and also with the constant gain POD controller when PFC is in the closed loop. These results are compared with the case when the system is performing without the PFC controller. From the results it is evident that the ANFIS based controller performance is better than the constant gain controller when the two controllers are in joint operation with the two choices of POD control signal, $\Delta U_{POD}=\Delta\delta_E$ *and* $\Delta\delta_B$. It is also observed the response is much improved in case of ANFIS based controller when $\Delta U_{POD}=\Delta\delta_E$. as in the case of POD-DVR control operation.

Figure 13 presents the simulation results on the system for a step rise in the reference power setting of the PFC controller. Simulation is done with step rise of 0.01 p.u mechanical power input of the machine at the time instant t = 0.5 second when the machine is operating in the nominal operating conditions. The performance of the ANFIS based POD controller with the PFC controller is examined for the control function of the PFC controller. The ΔP_e variations in the figure shows that with $\Delta U_{POD}=\Delta\delta_B$ the performance of PFC controller is similar for both the constant gain and the ANFIS trained POD controller. With $\Delta U_{POD}=\Delta\delta_E$, the constant gain POD is showing oscillatory response for the initial period and it takes nearly 5 seconds to attain the steady value, however with ANFIS trained POD the response is well damped.

Figure 14 shows the variations of$\Delta\omega$ of the synchronous machine with POD-PFC controllers in joint operation and also with ANFIS based POD-PFC controllers when the system is operating at load condition where P_e *and* Q_e values are higher than the nominal conditions and Figure 15 shows such responses with the equivalent reactance lower than the nominal value. When compared with the results obtained with POD controller alone it is evident that the ANFIS based controller is showing improved performance than constant gain controller for both the U_{POD} control signals considered. In all the cases considered the ANFIS based controller is

showing better response when the UPFC control signal $\Delta\delta_E$ is chosen.

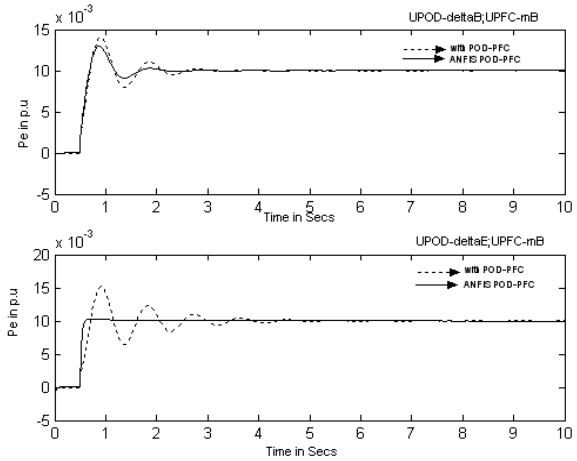

Fig. 13. ΔP_e variations for step change in P_{eref}.

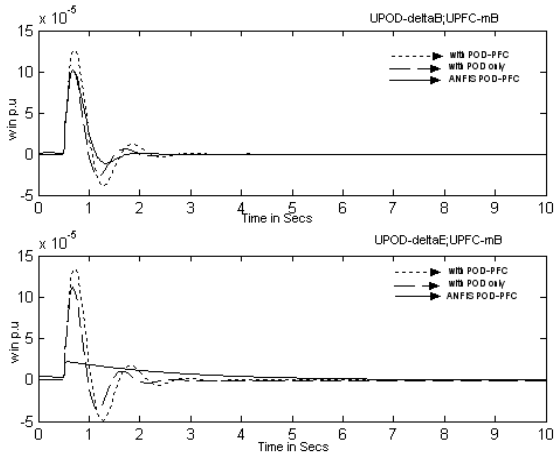

Fig. 14.comparison of $\Delta\omega$ variations for step change in mechanical power input *Pe=1.2p.u;Qe=0.3p.u*.

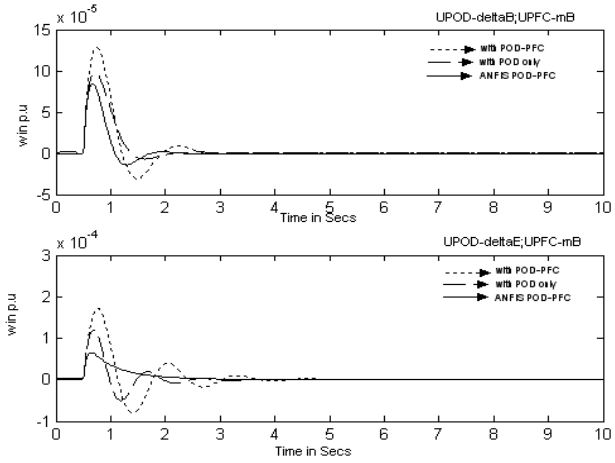

Fig. 15. comparison of $\Delta\omega$ variations for step change in mechanical power input *Pe=0.6p.u;Qe=0.1p.u ;Xe=0.3p.u*

5. CONCLUSION

Due to dynamic interactions among different UPFC controllers, performance is deteriorated when separately designed and individually implemented stable UPFC controllers are in joint operation. This paper has proposed an ANFIS based coordination controller for the UPFC to coordinate the POD controller with the control signals of other UPFC controllers. The ANFIS based adaptive controller is trained by the batch hybrid-learning rule and the training data is generated using the using phase compensation technique for design of POD controller.

The performance evaluation of the proposed controller for coordination with other controllers is done by conducting time domain simulations on linearized single machine infinite bus model of power system installed with UPFC in presence of DVR and PFC control channels considered separately with the chosen control output signals namely $\Delta U_{DVR}=\Delta\delta_E$ *and* $\Delta U_{PFC}=\Delta m_B$ .The

adaptive POD controller, which was adapted by a proper training data, is showing robust performance with the two choices of UPFC control signals,$\Delta U_{POD}=\Delta\delta_B$ *and* $\Delta\delta_E$ to variations in system loading and parameters. Investigations also illustrate the superiority of the proposed controller when compared to the constant gain controller under the different operating situations. In all the cases considered, the ANFIS based controller is showing better response when the UPFC control signal $\Delta\delta_E$ is chosen. This can be attributed to the better contribution of this signal to damping of electromechanical mode of oscillation as evident from the eigen value analysis results given in Table 3.

NOMENCLATURE

H : inertia constant
D : damping constant
T'_{do} : open circuit d-axis time constant
X_d : direct axis steady –state synchronous reactance of generator
X'_d : direct axis transient synchronous reactance of generator
X_q : quadrature axis steady –state synchronous reactance of generator
K_a : AVR gain
T_a : AVR time constant
X_{tE} : transformer reactance
X_E : reactance of excitation transformer (ET)
X_B : reactance of boosting transformer (BT)
X_{Bv} : transmission line reactance
X_e : equivalent reactance of the system
P_e : real power output
Q_e : reactive power output
V_t : generator terminal voltage
m_E : modulating index of shunt converter
m_B : modulating index of series converter
δ_E : phase angle of shunt converter voltage
δ_B : phase angle of series converter voltage
C_{dc} : dc link capacitance
V_{dc} : dc link voltage

REFERENCES

[1] Hingorani, N.G. 1988. Power Electronics in Electrical Utilities. *IEEE Proceedings* 76(4): 481-482.

[2] Gyugyi, L., and Schauderetat, C.D. 1995. The unified power flow controller: A new approach to power transmission control. *IEEE Transactions on Power Delivery* 10(2): 1085 – 1097.

[3] Nabavi-Niaki, A., and Iravani, M.R. 1996. Steady-state and dynamic models of unified power flow controller for power system studies. *IEEE Transactions on Power Systems* (11): 1937-43.

[4] Papic, I., Zunko, P., Povh, D., and Weinhold, M. 1997. Basic control of unified power flow controller. *IEEE Transactions on Power Systems* 12(4): 1734-39.

[5] Smith, K.S., Ran, L., and Penman, J. 1997. Dynamic modeling of unified power flow controller. *IEE Proceedings on Generation, Transmission and Distribution* 144(1): 7-12.

[6] Wang, H.F. 2002. Interactions and multivariable design of multiple control functions of a unified power flow controller. *Electrical Power and Energy Systems* 24: 591-600.

[7] Tambey, N., and Kothari, M.L. 2003. Unified Power Flow Controller based damping controllers for damping low frequency oscillations in Power System. *Journal of Institution of Engineers – Electrical* 84: 35-41.

[8] Tambey, N., and Kothari, M.L. 2003. Damping of power system oscillations with UPFC. *IEE Proceedings on General Transmission Distribution* 150(2): 129-140.

[9] Chang, C-T., and Hsu, Y-Y. 2003. Design of an ANN tuned adaptive UPFC supplementary damping controller for power system dynamic performance enhancement. *Electric Power System Research* 66: 259-65.

[10] Jang, J.S.R.1993. ANFIS: Adaptive-Network-Based Fuzzy Inference System. *IEEE Transactions on Systems, Man and Cybernetics* 23(3): 665-685.

[11] Wang, H.F. 1999. Damping function of unified power flow controller. *IEE Proceedings on General Transmission Distribution* 146(1): 81-87.

[12] IEEE Power Engineering Society. 1992. IEEE Recommended Practice for Excitation System Models for Power System Stability Studies. *IEEE Standard* 421.5.

[13] Terond, C. 1998. Modeling of power electronics equipments (FACTS) in load flow and stability programs: A representation guide for power system planning and analysis. Paris, *Technical Report CIGRE* TF 38-01-08, September.

[14] Wang, H.F., Li, M. and Swift, F.J. 1997. FACTS – based stabilizer designed by the phase compensation method. In *Proceedings on APSCOM Part I and Part II,* Hong Kong: 638-649.

[15] Hang, C.C., Astrom, K.J. and Ho, W.K. 1991. Refinements of the Ziegler- Nichols tuning formula. *IEE Proceedings-Control Theory and Applications* 138(2): 111-118.

[16] Tagaki, T., and Sugeno, M. 1985. Fuzzy identification of systems and its applications to modeling and control. *IEEE Transactions on Systems, Man, and Cybernetics* 15: 116-132.

APPENDIX

A. System Data

Synchronous Machine:
$H= 4.0$ s, $D=0.0$, $T'_{do}= 5.044$ s, $X_d=1.0$ p.u
$X'_d=0.3$ p.u, $X_q= 0.6$ p.u

Excitation system: $K_a=100$, $T_a=0.01$ s

Transformer and Transmission line
$X_{tE}=0.1$ p.u , $X_E=0.1$ p.u , $X_B= 0.1$ p.u , $X_{Bv}=0.3$ p.u
$X_e=0.5$ p.u

Nominal operating condition:
$P_e=0.6$ p.u , $Q_e=0.1$ p.u , $V_t=1.0$ p.u ,$f=60$Hz

UPFC parameters

m_E =0.4 , m_B =0.08, δ_E =-85.3° , δ_B =-78.2°, V_{dc} =2 p.u C_{dc}

B. K constants calculated for the nominal operating conditions

k_1 = 1.3417	k_2 = 0.1348	k_3 = 2.4848	k_4 = 0. 4428
k_5 = -0.1454	k_6 = 0.3431	k_7 = 0.1795	k_8 = 0.0443
k_9 = 0.0006	k_{pd} = .0719	k_{vd} =-0.0911	k_{qd} = 0.2285
k_{pe} = 0.1543	k_{pb} =0.1259	$k_{p\delta e}$ =0.5229	$k_{p\delta b}$ = .0377
k_{qe} = 0.5286	k_{qb} =0.2077	$k_{q\delta e}$ = -.0173	$k_{q\delta b}$ =-.0308
k_{ve} = -0.2110	k_{vb} =-.0812	$k_{v\delta e}$ =0.0093	$k_{v\delta b}$ = 0.0135
k_{ce} = -0.0156	k_{cb} =0.0715	$k_{c\delta e}$ = -.2252	$k_{c\delta b}$ = -.055